Existence of a dynamic compensation temperature of a mixed spin-2 and spin-5/2 Ising ferrimagnetic system in an oscillating field

Mustafa Keskin[1,*] and Mehmet Ertaş[2,†]
[1]*Department of Physics, Erciyes University, 38039 Kayseri, Turkey*
[2]*Institute of Science, Erciyes University, 38039 Kayseri, Turkey*
(Received 11 July 2009; published 30 December 2009)

The magnetic properties of a nonequilibrium mixed spin-2 and spin-5/2 Ising ferrimagnetic system with a crystal-field interaction (D) in the presence of a time-varying magnetic field on a hexagonal lattice are studied by using the Glauber-type stochastic dynamics. The model system consists of two interpenetrating sublattices with $\sigma=2$ and $S=5/2$. The Hamiltonian model includes intersublattice, intrasublattice, and crystal-field interactions. The intersublattice interaction is considered antiferromagnetic to have a simple but interesting model of a ferrimagnetic system. The set of mean-field dynamic equations is obtained by employing the Glauber transition rates. First, we investigate the time variations in average sublattice magnetizations to find the phases in the system, and the temperature dependence of the dynamic sublattice magnetizations to characterize the nature (continuous or discontinuous) of the phase transitions and to obtain the dynamic phase transition points. Then, we study the temperature dependence of the total magnetization to find the dynamic compensation points as well as to determine the type of behavior. We also investigate the effect of a crystal-field interaction and the exchange couplings between the nearest-neighbor pairs of spins on the compensation phenomenon and present the dynamic phase diagrams. According to values of Hamiltonian parameters, the paramagnetic, the nonmagnetic, and the four different ferrimagnetic fundamental phases, seven different mixed phases, and the compensation temperature, or the *N*-type behavior in the Néel classification nomenclature exist in the system. A comparison is made with the results of the available mixed spin Ising systems.

DOI: 10.1103/PhysRevE.80.061140 PACS number(s): 05.50.+q, 05.70.Fh, 75.10.Hk, 75.40.Mg

I. INTRODUCTION

In recent years, the phenomenon of ferrimagnetism has been one of the intensively studied subjects in statistical mechanics and condensed matter physics, because of their potential device applications in technologically important materials. In contrast to ferromagnets and antiferromagnets, there is in ferrimagnets an important possibility of the existence, under certain conditions, of a compensation temperature where the total magnetization vanishes below the critical temperature. The existence of compensation temperatures is of great technological importance, since at this point only a small driving field is required to change the sign of the total magnetization. This property is very useful in thermomagnetic recording, electronic, and computer technologies. On the other hand, mixed Ising systems provide simple models that can show ferrimagnetic ordering and they may have compensation temperatures. Moreover, since the mixed-spin Ising systems have less translational symmetry than their single spin counterparts, they exhibit many phenomena that cannot be observed in the single-spin Ising systems and the study of these systems can be relevant for understanding of bimetallic molecular systems based magnetic materials. One of the earliest and most extensively studied mixed spin Ising systems is the spin-2 and spin-5/2 mixed system besides the mixed spins Ising systems with spins (1, 1/2) (see [1–15] and references therein), with spins (1/2, 3/2) (see [16–23] references therein), with spins (1, 3/2) (see [24–30] references therein).

An early attempt to study the mixed spin-2 and spin-5/2 system on a honeycomb lattice was made by Kaneyoshi and co-workers [31] within the frame work of the effective field theory (EFT). In particular, they examined the effect of a positive single-ion anisotropy on the compensation temperature in order to clarify the characteristic feature of the temperature dependence of the total magnetization observed for a molecular-based magnetic material, $N(n\text{-}C_4H_9)_4Fe^{II}Fe^{III}(C_2O_4)_3$ with $\sigma=2$ (Fe^{II}) and $S=5/2$ (Fe^{III}). Nakamura [32,33] applied to Monte Carlo (MC) simulations to study the magnetic properties of a mixed spin-2 and spin-5/2 system on a honeycomb lattice in order to investigate a characteristic feature of $AFe^{II}Fe^{III}(C_2O_4)_3$ $[A=N(n\text{-}C_nH_{2n+1})_4]$ [32] and the effect of single-ion anisotropy on the characteristic feature of the temperature dependence of the total magnetization [33]. Nakamura [34] also studied the magnetic properties of the mixed spin-2 and spin-5/2 system on a layered honeycomb lattice with MC simulations in order to clarify the characteristic behavior of $AFe^{II}Fe^{III}$ $(C_2O_4)_3$ $[A=N(n\text{-}C_nH_{2n+1})$, $n=3-5]$, especially the effect of the interlayer interactions and a single-ion anisotropy on the existence of the compensation point were examined. Li and co-workers [35,36] studied the magnetic properties of the mixed spin-2 and spin-5/2 system on a layered honeycomb lattice by a multisublattice Green's function technique to investigate the magnetic behavior of $AFe^{II}Fe^{III}$ $(C_2O_4)_3$ $[A=N(n\text{-}C_nH_{2n+1})$, $n=3-5]$ [35] and the compensation behavior of the system [36]. They [37] also studied the low-temperature properties of the mixed spin-2 and spin-5/2 Heisenberg ferromagnetic system on a honeycomb lattice by using a linear spin-wave theory in order to clarify the low-temperature behavior of $AFe^{II}Fe^{III}$ $(C_2O_4)_3$ [*A*

*keskin@erciyes.edu.tr
†mehmetertas@erciyes.edu.tr

$=N(n\text{-}C_nH_{2n+1})$, $n=3-5$]. Wei and co-workers [38,39] examined the internal energy, specific heat and initial susceptibility [38], and tricritical behavior [39] of the mixed spin-2 and spin-5/2 ferrimagnetic system with an interlayer coupling by the use of the EFT with correlations. Recently, Albayrak and co-workers [40] studied the critical behavior of the mixed spin-2 and spin-5/2 Ising ferromagnetic system on Bethe lattice by using the exact recursion equations.

Despite these equilibrium studies, as far as we know, the nonequilibrium aspects of the mixed spin-2 and spin-5/2 Ising ferrimagnetic system have not been investigated. Therefore, the purpose of the present work is to study the magnetic properties of a nonequilibrium mixed spin-2 and spin-5/2 Ising ferrimagnetic system on a hexagonal lattice with a crystal-field interaction in the presence of a time-dependent oscillating external magnetic field. We use the Glauber-type stochastic dynamics [41] to describe the time evolution of the system. We examine the time variations in average sublattice magnetizations to find the phases in the system, and the thermal behavior of the dynamic magnetizations to characterize the nature (continuous or discontinuous) of the phase transitions and obtain the dynamic phase transition (DPT) points. We investigate the total dynamic magnetization as a function of the temperature to find the dynamic of compensation temperatures as well as to determine the type of behavior. We also investigate the effect of the interactions parameters on the compensation phenomenon. From these studies, the existence of the dynamic compensation temperatures is investigated and dynamic phase diagrams are calculated. A comparison is made with the results of the available mixed spin Ising systems.

The outline of the rest of the paper is follows. In Sec. II, the model is presented briefly and the derivation of the mean-field dynamic equations of motion is given by using the Glauber-type stochastic dynamics in the presence of a time-varying magnetic field. In Sec. III, the behavior of the average sublattice magnetizations, dynamic sublattice magnetizations and dynamic total magnetization are studied in detail, and the dynamic phase diagrams are presented. Finally, we give the summary and conclusion in the last section.

II. MODEL AND EQUATIONS OF MOTIONS

We consider a mixed spin-2 and spin-5/2 Ising ferrimagnetic system on a hexagonal lattice. The lattice is formed by alternate layers of σ and S spins; hence, the two different types of spins are described by Ising variables, which can take the values $\sigma=\pm 2,\pm 1,0$ and $S=\pm 5/2,\pm 3/2,\pm 1/2$. σ and S spins are distributed in alternate layers of a hexagonal lattice, seen in Fig. 1. In Fig. 1, open and solid circles represent σ and S spin, respectively. The Hamiltonian model for the system is

$$H=-J_1\sum_{\langle ij\rangle}\sigma_i S_j-J_2\sum_{\langle ij\rangle}\sigma_i\sigma_j-J_3\sum_{\langle ij\rangle}S_iS_j-D\left(\sum_i\sigma_i^2+\sum_j S_j^2\right)-H\left(\sum_i\sigma_i+\sum_j S_j\right), \quad (1)$$

where the summation index $\langle ij\rangle$ denotes a summation over all pairs of nearest-neighbor spins. J_1, J_2, and J_3 are the exchange couplings between the nearest-neighbor pairs of spins $\sigma-S$, $\sigma-\sigma$, and S-S, respectively. It is seen from Fig. 1, J_1 the interaction is restricted to the z_1 nearest-neighbor pair of spins that $z_1=4$, and J_2 and J_3 are restricted to the coordination numbers of z_2 and z_3, respectively, in which $z_2=z_3=2$. The parameter J_1 will be taken negative in all the subsequent analyses, that is, the intersublattice coupling is antiferromagnetic to have a simple but an interesting model of a ferrimagnetic system. D is the crystal-field interaction or a single-ion anisotropy constant. We take the same single-ion anisotropy constant for both magnetic moments in order to avoid one more interaction constant, as in Refs. [42,43]. One can also use the different anisotropy constants for both magnetic moments as in Refs. [27,28,36,38,39]. H is an oscillating magnetic field of the form

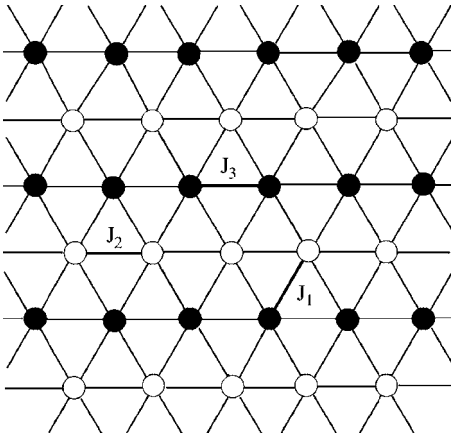

FIG. 1. The sketch of the spin arrangement on the hexagonal lattice. The lattice is formed by alternate layers of σ (open circles) and S (solid circles) spins.

$$H(t)=H_0\cos(\mathrm{wt}), \quad (2)$$

where H_0 and $w=2\pi\nu$ are the amplitude and the angular frequency of the oscillating field, respectively. The system is in contact with an isothermal heat bath at absolute temperature T_A.

Now, we apply the Glauber-type stochastic dynamics [41] to obtain the set of mean-field dynamic equations. Thus, the system evolves according to the Glauber-type stochastic process at a rate of $1/\tau$ transitions per unit time; hence the frequency of spin flipping, f, is $1/\tau$. Leaving the S spins fixed, we define $P^{\sigma}(\sigma_1,\sigma_2,\ldots,\sigma_N;t)$ as the probability that the system has the $\sigma-$ spin configuration, $\sigma_1,\sigma_2,\ldots,\sigma_N$, at time t, also, by leaving the $\sigma-$ spins fixed, we define $P^{S}(S_1,S_2,\ldots,S_N;t)$ as the probability that the system has the S-spin configuration, $S_1,S_2,\ldots,S_N$, at time t. Then, we calculate $W_i^{\sigma}(\sigma_i\rightarrow\sigma_i')$ and $W_j^{S}(S_j\rightarrow S_j')$, the probabilities per unit time that the ith σ spin changes from σ_i to σ_i' (while the S spins momentarily fixed) and the jth S spin changes from S_j to S_j' (while the σ spins momentarily fixed), respectively. Thus, if the S spins momentarily fixed, the master equation for the σ spins can be written as

$$\frac{d}{dt}P^{\sigma}(\sigma_1,\sigma_2,\ldots,\sigma_N;t) = -\sum_i \left[\sum_{\sigma_i\neq\sigma_i'} W_i^{\sigma}(\sigma_i\to\sigma_i')\right] \times P^{\sigma}(\sigma_1,\sigma_2,\ldots,\sigma_i,\ldots\sigma_N;t) + \sum_i \left[\sum_{\sigma_i\neq\sigma_i'} W_i^{\sigma}(\sigma_i'\to\sigma_i)\right] \times P^{\sigma}(\sigma_1,\sigma_2,\ldots,\sigma_i',\ldots\sigma_N;t), \tag{3}$$

where $W_i^{\sigma}(\sigma_i\to\sigma_i')$ is the probability per unit time that the ith spin changes from the value σ_i to σ_i'. Since the system is in contact with a heat bath at absolute temperature T_A, each spin can change from the value σ_i to σ_i' with the probability per unit time;

$$W_i^{\sigma}(\sigma_i\to\sigma_i') = \frac{1}{\tau}\frac{\exp[-\beta\Delta E^{\sigma}(\sigma_i\to\sigma_i')]}{\sum_{\sigma_i'}\exp[-\beta\Delta E^{\sigma}(\sigma_i\to\sigma_i')]}, \tag{4}$$

where $\beta=1/k_B\,T_A$, k_B is the Boltzmann constant and T_A is the absolute temperature, $\Sigma_{\sigma_i'}$ is the sum over the five possible values of $\sigma_i'=\pm 2,\pm 1,0$, and

$$\Delta E^{\sigma}(\sigma_i\to\sigma_i') = -(\sigma_i'-\sigma_i)\left(J_1\sum_j S_j + J_2\sum_j \sigma_j + H\right) - [(\sigma_i')^2-(\sigma_i)^2]D, \tag{5}$$

gives the change in the energy of the system when the σ_i spin changes. The probabilities $W_i^{\sigma}(\sigma_i\to\sigma_i')$ are given in the Appendix. The probabilities satisfy the detailed balance condition. Since $W_i^{\sigma}(\sigma_i\to\sigma_i')$ does not depend on the value σ_i, we can write $W_i^{\sigma}(\sigma_i\to\sigma_i')=W_i^{\sigma}(\sigma_i')$, then the master equation becomes

$$\frac{d}{dt}P^{\sigma}(\sigma_1,\sigma_2,\ldots,\sigma_N;t) = -\sum_i \left[\sum_{\sigma_i\neq\sigma_i'} W_i^{\sigma}(\sigma_i')\right] P^{\sigma}(\sigma_1,\sigma_2,\ldots,\sigma_i,\ldots,\sigma_N;t) + \sum_i W_i^{\sigma}(\sigma_i)\left[\sum_{\sigma_i\neq\sigma_i'} P^{\sigma}(\sigma_1,\sigma_2,\ldots,\sigma_i',\ldots,\sigma_N;t)\right]. \tag{6}$$

Since the sum of the probabilities is normalized to one, by multiplying both sides of Eq. (6) by σ_k and taking the average, we obtain

$$\tau\frac{d}{dt}\langle\sigma_k\rangle = -\langle\sigma_k\rangle + \left\langle \frac{2\exp(4\beta D)\sinh\left[2\beta\left(J_1\sum_j S_j + J_2\sum_j\sigma_j + H\right)\right] + \exp(\beta D)\sinh\left[\beta\left(J_1\sum_j S_j + J_2\sum_j\sigma_j + H\right)\right]}{\exp(4\beta D)\cosh\left[2\beta\left(J_1\sum_j S_j + J_2\sum_j\sigma_j + H\right)\right] + \exp(\beta D)\cosh\left[\beta\left(J_1\sum_j S_j + J_2\sum_j\sigma_j + H\right)\right] + \frac{1}{2}}\right\rangle, \tag{7}$$

or, in terms of a mean field approach,

$$\tau\frac{d}{dt}\langle\sigma\rangle = -\langle\sigma\rangle + \left\langle \frac{2\exp(4\beta D)\sinh(2\beta a_1) + \exp(\beta D)\sinh(\beta a_1)}{\exp(4\beta D)\cosh(2\beta a_1) + \exp(\beta D)\cosh(\beta a_1) + \frac{1}{2}}\right\rangle, \tag{8}$$

where $\langle\ldots\rangle$ denotes the canonical thermal average and $a_1=[J_1z_1\langle S\rangle + J_2z_2\langle\sigma\rangle + H_0\cos(\mathrm{wt})]$. Equation (8) can be written in the form

$$\Omega\frac{d}{d\xi}m_{\sigma} = -m_{\sigma} + \left\langle \frac{2\exp\left(4\frac{d}{T}\right)\sinh\left(2\frac{a_2}{T}\right) + \exp\left(\frac{d}{T}\right)\sinh\left(\frac{a_2}{T}\right)}{\exp\left(4\frac{d}{T}\right)\cosh\left(2\frac{a_2}{T}\right) + \exp\left(\frac{d}{T}\right)\cosh\left(\frac{a_2}{T}\right) + \frac{1}{2}}\right\rangle, \tag{9}$$

where $T=\frac{k_BT_A}{|J_1|}$, $d=\frac{D}{|J_1|}$, $a_2=(-z_1m_S+\frac{J_2}{|J_1|}z_2m_{\sigma}+\mathrm{h}_0\cos(\xi))$, $\mathrm{h}_0=\frac{H_0}{|J_1|}$, $m_{\sigma}=\langle\sigma\rangle$, $m_S=\langle S\rangle$, $\xi=\mathrm{wt}$, and $\Omega=\tau\mathrm{w}$.

Now, assuming that the spins σ remain momentarily fixed and S spins change, we obtain the second mean-field dynamic equation by using a similar calculation as

$$\Omega\frac{d}{d\xi}m_S = -m_S + \left\langle \frac{5\exp\left(2\frac{d}{T}\right)\sinh\left(\frac{5}{2}\frac{a_3}{T}\right) + 3\exp\left(-2\frac{d}{T}\right)\sinh\left(\frac{3}{2}\frac{a_3}{T}\right) + \exp\left(-4\frac{d}{T}\right)\sinh\left(\frac{1}{2}\frac{a_3}{T}\right)}{2\exp\left(2\frac{d}{T}\right)\cosh\left(\frac{5}{2}\frac{a_3}{T}\right) + 2\exp\left(-2\frac{d}{T}\right)\cosh\left(\frac{3}{2}\frac{a_3}{T}\right) + \exp\left(-4\frac{d}{T}\right)\cosh\left(\frac{1}{2}\frac{a_3}{T}\right)}\right\rangle, \tag{10}$$

where $a_3=(-z_1 m_\sigma+\frac{J_3}{|J_1|}z_3 m_S+\mathrm{h}_0\cos(\xi))$. Hence, a set of mean-field dynamical equations of the system is obtained. We fixed $J_1=-1$ that the intersublattice interaction is antiferromagnetic and $\Omega=2\pi$. In the next section, we will give the numerical results of these equations.

III. NUMERICAL RESULTS AND DISCUSSIONS

A. Time variations in average order parameters

In order to investigate the behaviors of time variations in order parameters, first, we have to study the stationary solutions of the set of coupled mean-field dynamical equations, given in Eqs. (9) and (10), when the parameters T, J_2, J_3, d, and h_0 are varied. The stationary solutions of these equations will be periodic functions of ξ with period 2π; that is, $m_\sigma(\xi+2\pi)=m_\sigma(\xi)$ and $m_S(\xi+2\pi)=m_S(\xi)$. Moreover, they can be one of three types according to whether they have or do not have the property

$$m_\sigma(\xi+\pi)=-m_\sigma(\xi) \tag{11a}$$

and

$$m_S(\xi+\pi)=-m_S(\xi). \tag{11b}$$

The first type of solution satisfies both Eqs. (11a) and (11b) and is called a symmetric solution, which corresponds to a paramagnetic (p) phase. In this solution, the sublattice average magnetizations, $m_\sigma(\xi)$ and $m_S(\xi)$, are equal to each other. They oscillate around the zero value and are delayed with respect to the external magnetic field. The second type of solution, which does not satisfy Eqs. (11a) and (11b), is called a nonsymmetric solution, but this solution corresponds to a ferrimagnetic (i) solution because the sublattice average magnetizations $m_\sigma(\xi)$ and $m_S(\xi)$ are not equal each other $[m_\sigma(\xi)\neq m_S(\xi)]$ and they oscillate around a nonzero value. Hence, if $m_\sigma(\xi)$ and $m_S(\xi)$ oscillate around ± 2 and $\pm 5/2$, respectively, this solution called the ferrimagnetic-1 (i_1) phase; if $m_\sigma(\xi)$ and $m_S(\xi)$ oscillate around ± 2 and $\pm 3/2$, respectively, the solution called the ferrimagnetic-2 (i_2) phase; if $m_\sigma(\xi)$ and $m_S(\xi)$ oscillate around ± 2 and $\pm 1/2$, respectively, the solution called the ferrimagnetic-3 (i_3) phase, and if $m_\sigma(\xi)$ and $m_S(\xi)$ oscillate around ± 1 and $\pm 1/2$, respectively, the solution called the ferrimagnetic-4 (i_4) phase. The third type of solution, which satisfies Eq. (11a) but does not satisfy Eq. (11b), corresponds to a nonmagnetic solution (nm). In this case, $m_\sigma(\xi)$ oscillates around the zero value and is delayed with respect to the external magnetic field and $m_S(\xi)$ does not follow the external magnetic field anymore, but instead of oscillating around a zero value, it oscillates around a nonzero value. These facts are seen explicitly by solving Eqs. (9) and (10), numerically. These equations are solved by using the numerical method of the Adams-Moulton predictor corrector method for a given set of parameters and initial values. A few explanatory examples are given in Fig. 2. Figures 2(a)–2(d) represent the paramagnetic, ferrimagnetic-1, nonmagnetic fundamental solutions or phases, and the i_4+p mixed phase, respectively. In addition to these three fundamental phases and a mixed phase, three more fundamental phases, namely, the ferrimagnetic-2 (i_2), the ferrimagnetic-3 (i_3), the ferrimagnetic-4 (i_4), and six more mixed phases, namely, the i_1+p in which i_1, p solutions coexist; the i_1+nm in which i_1, nm solutions coexist; the i_2+p in which i_2, p solutions coexist; the i_2+nm in which i_2, nm solutions coexist; the i_3+p in

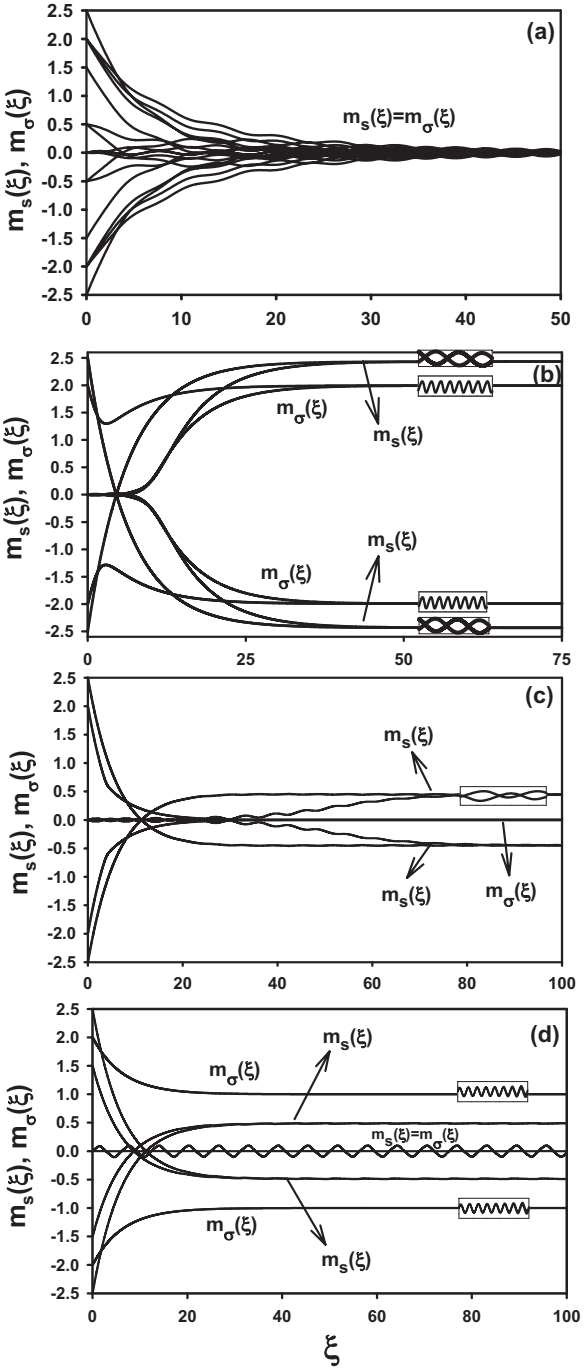

FIG. 2. Time variations in the average sublattice magnetizations $[m_\sigma(\xi)$ and $m_S(\xi)]$: (a) exhibiting a paramagnetic phase (p), $J_1=-1.0$, $J_2=2.0$, $J_3=0.7$, $d=-4.5$, $\mathrm{h}_0=2.5$, and $T=18$. (b) Exhibiting a ferrimagnetic phase (i_1), $J_1=-1.0$, $J_2=2.0$, $J_3=0.1$, $d=1$, $\mathrm{h}_0=0.1$, and $T=4$. (c) Exhibiting a nonmagnetic phase (nm), $J_1=-1.0$, $J_2=1.2$, $J_3=0.5$, $d=-3$, $\mathrm{h}_0=0.1$, and $T=0.15$. (d) Exhibiting a coexistence region or mixed phase (i_4+p), $J_1=-1.0$, $J_2=8.0$, $J_3=0.5$, $d=-10$, $\mathrm{h}_0=2.5$, and $T=1.2$.

which i_3, p solutions coexist and the i_4+nm in which i_4, nm solutions coexist mixed phases, exist in the system.

B. Thermal behavior of dynamic sublattice magnetizations and the total magnetization

First, we investigate the behavior of the average sublattice magnetizations in a period or the dynamic sublattice magnetizations as a function of the reduced temperature. This investigation leads us to characterize the nature (a first order or a second order) of phase transitions and find the DPT. Then, we study the total dynamic magnetization as a function of temperature to find the compensation temperatures and to determine the type of behavior. The dynamic sublattice magnetizations $(\mathrm{M}_\sigma, \mathrm{M}_S)$ and the total dynamic magnetization $\mathrm{M}_t = \frac{\mathrm{M}_\sigma(\xi)+\mathrm{M}_s(\xi)}{2}$ are defined as

$$\mathrm{M}_\sigma = \frac{1}{2\pi}\int_0^{2\pi} m_\sigma(\xi)d\xi, \tag{12a}$$

$$\mathrm{M}_S = \frac{1}{2\pi}\int_0^{2\pi} m_S(\xi)d\xi, \tag{12b}$$

$$\mathrm{M}_t = \frac{1}{2\pi}\int_0^{2\pi} \left(\frac{m_S(\xi)+m_\sigma(\xi)}{2}\right)d\xi. \tag{12c}$$

The behaviors of dynamic sublattice magnetizations $(\mathrm{M}_\sigma, \mathrm{M}_S)$ and the total dynamic magnetization (M_t) as functions of the temperature for several values of interaction parameters are obtained by combining numerical methods of the Adams-Moulton predictor corrector with the Romberg integration. The total magnetization (M_t) vanishes at the compensation temperature T_{comp}. Then, the compensation point can be determined by looking for the crossing point between the absolute values of the sublattice magnetizations. Therefore, at the compensation point, we must have

$$|\mathrm{M}_\sigma(T_{\mathrm{comp}})| = |\mathrm{M}_S(T_{\mathrm{comp}})| \tag{13}$$

and

$$\mathrm{sgn}[\mathrm{M}_\sigma(T_{\mathrm{comp}})] = -\,\mathrm{sgn}[\mathrm{M}_S(T_{\mathrm{comp}})]. \tag{14}$$

We also require that $T_{\mathrm{comp}} < T_c$, where T_c is the critical point temperature. These conditions demonstrate that at T_{comp}, the M_σ and M_S cancel each other, whereas at T_c both are zero. Few explanatory and interesting examples are plotted in Figs. 3(a)–3(e) in order to illustrate the calculation of the DPT points and the compensation temperatures. In these figures, T_c and T_t are the critical or the second-order and first-order phase transition temperatures, respectively. Figure 3(a) shows the behavior of $|\mathrm{M}_\sigma|$, $|\mathrm{M}_S|$, and $|\mathrm{M}_t|$ as a function of the temperature for $J_1=-1.0$, $J_2=3.0$, $J_3=0.8$, $d=-1.0$, and $\mathrm{h}_0=0.1$. In Fig. 3(a), $|\mathrm{M}_\sigma|=2$ and $|\mathrm{M}_S|=2.5$ at the zero temperature, and they decrease to zero continuously until T_c as the temperature increases, hence a second-order phase transition occurs at $T_c=16.96$. In this case, the dynamic phase transition is from the i_1 phase to the p phase. Moreover, from the behavior of the total dynamic magnetization, one can see that only one compensation temperature or N-type behavior occurs in the system that exhibits the same behavior classified after Néel [44] theory as the N-type [45]. Figures 3(b) and 3(c) illustrate the thermal variations of $|\mathrm{M}_\sigma|$, $|\mathrm{M}_S|$, and $|\mathrm{M}_t|$ for $J_1=-1.0$, $J_2=2.0$, $J_3=0.2$, $d=-1.5$, and $\mathrm{h}_0=0.1$ for various different initial values. The behavior of Fig. 3(b), is similar to Fig. 3(a), hence the system undergoes a second-order phase transition from the i_1 phase to the p phase at $T_c=11.29$. In Fig. 3(c), the system undergoes two successive phase transitions: the first one is a first order, because the discontinuous occurs for the dynamic sublattice magnetizations at $T_t=0.36$. Transition is from the p phase to the i_1 phase. The second one is a second order from the i_1 phase to the p phase at $T_c=11.29$. This means that the coexistence region, i.e., the i_1+p mixed phase exist in the system. Moreover, the compensation temperature or the N-type behavior exists in the system again. We should also mention that two successive transitions have also been experimentally observed in $DyVO_4$ [46]. Finally, Figs. 3(d) and 3(e) show the behavior the thermal variations of $|\mathrm{M}_\sigma|$, $|\mathrm{M}_S|$, and $|\mathrm{M}_t|$ for $J_1=-1.0$, $J_2=8.0$, $J_3=0.1$, $d=-10.0$, and $\mathrm{h}_0=2.5$ for various different initial values. In Fig. 3(d), $|\mathrm{M}_\sigma|=1$ and $|\mathrm{M}_S|=0.5$ at the zero temperature and they decrease zero discontinuously as the temperature increases; hence the system undergoes a first-order phase transition from the i_4 phase to the p phase at $T_t=2.52$. In Fig. 3(e), $|\mathrm{M}_\sigma|$, $|\mathrm{M}_S|$, and $|\mathrm{M}_t|$ always equal to zero; hence the system does not undergo any phase transition. This figure corresponds to the p phase. From Figs. 3(d) and 3(e), one can see that the i_4+p mixed phase region exists until T_t. There is no compensation temperature in the system for this case.

C. Dynamic phase diagrams

Since we have obtained DPT points and compensation temperatures in Sec. III B, we can now present the dynamic phase diagrams of the system. The calculated phase diagrams in the (d,T) plane are presented in Fig. 4 and (J_2,T), $(-J_3,T)$, (d,J_2), and $(d,-J_3)$ planes are presented in Fig. 5 for various values of interaction parameter. In these dynamic phase diagrams, the solid, dashed, and dash-dot-dot lines represent the second-order, first-order phase transitions temperatures, and the compensation temperatures, respectively. The dynamic tricritical point is denoted by a filled circle.

Figure 4 illustrates the dynamic phase diagrams including the compensation behaviors in (d,T) plane and seven main topological different types of phase diagrams are seen. From these phase diagrams, the following phenomena have been observed. (1) Fig. 4(a) does not contain the compensation temperatures, but the others do. (2) The re-entrant behavior is only seen in the phase diagrams of Figs. 4(a), 4(c)–4(e), and 4(g). (3) The system contains the p, nm, i_1 and i_2 fundamental phases, and the i_1+p, i_2+p, i_4+p, i_1+nm, and i_4 +nm mixed phases. (4) The system exhibits one or two the dynamic triple point (TP), seen in Figs. 4(e)–4(g). Moreover, a dynamic quadruple point (QP) appears in Fig. 4(g). (5) In Fig. 4(f), the filled triangle separates the i_2 phase from the i_1 for high value of T and the i_2+p mixed phase from the i_1 $+p$ mixed phase for low value of T. We have found a similar behavior to the one seen in the equilibrium phase diagrams

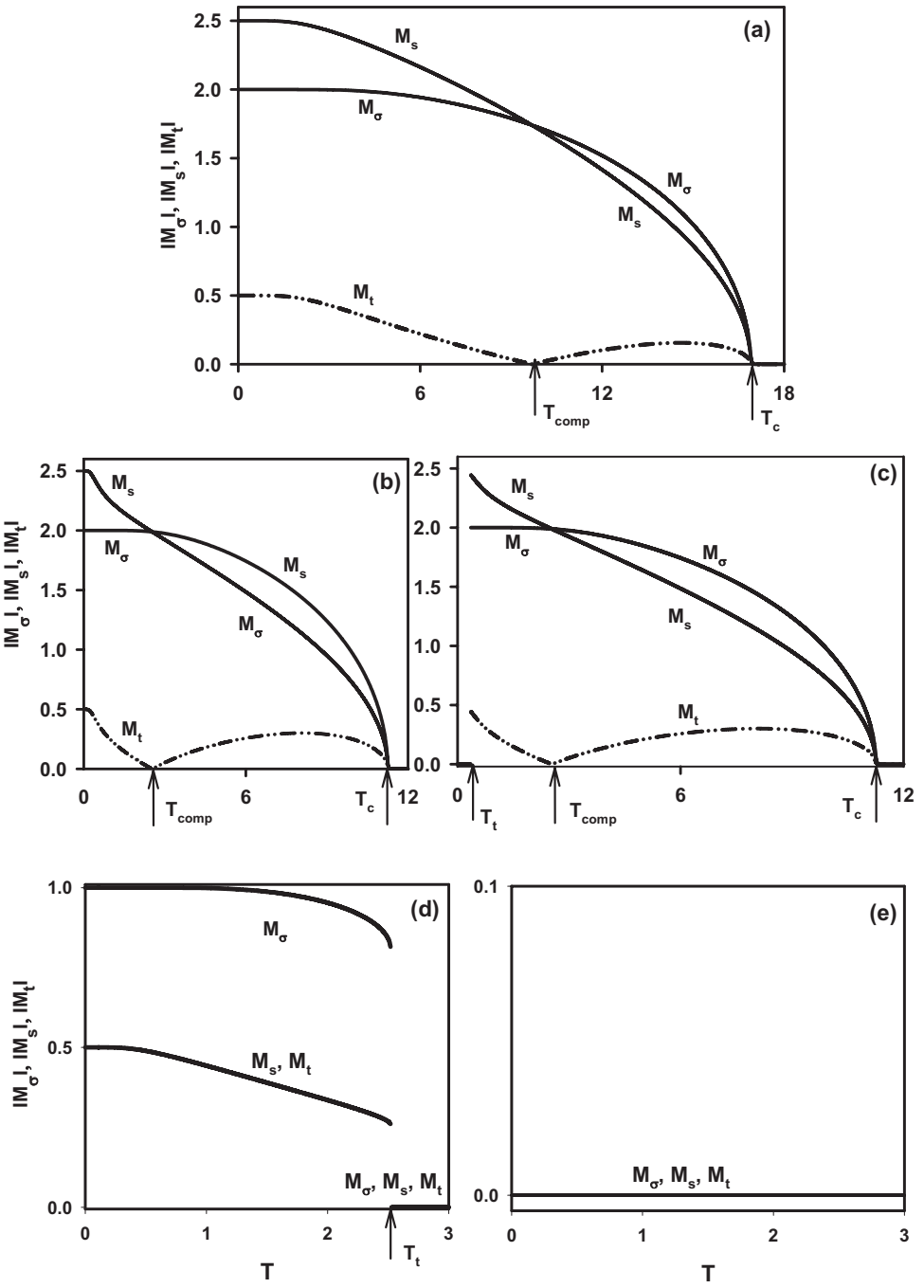

FIG. 3. The temperature dependence of the dynamic sublattice magnetizations ($|M_\sigma|, |M_S|$) and the total dynamic magnetization ($|M_t|$). T_c and T_t are the second- and first-order phase transition temperatures, respectively. (a) Exhibiting a second-order phase transition from the i_1 phase to the p phase for $J_1=-1.0$, $J_2=3.0$, $J_3=0.8$, $d=-1.0$, and $h_0=0.1$ and T_c is found 16.96. (b) Exhibiting a second-order phase transition from the i_1 phase to the p phase for $J_1=-1.0$, $J_2=2.0$, $J_3=0.2$, $d=-1.5$, and $h_0=0.1$ and the initial values of $|M_\sigma|$ and $|M_S|$ are taken one; T_c is found 11.29. (c) Exhibiting two successive phase transitions, the first one is a first-order phase transition from the p phase to the i_1 phase and the second one is a second-order phase transition the from the i_1 phase to the p phase for $J_1=-1.0$, $J_2=2.0$, $J_3=0.2$, $d=-1.5$, and $h_0=0.1$ and the initial values of $|M_\sigma|$ and $|M_S|$ are taken zero; T_c and T_t are found 11.29 and 0.36, respectively. (d) Exhibiting a first-order phase transition from the i_4 phase to the p phase for $J_1=-1.0$, $J_2=8.0$, $J_3=0.1$, $d=-10$, and $h_0=2.5$ and the initial values of $|M_\sigma|$ and $|M_S|$ are taken one; T_t is found 2.52. (e) The system does not undergo any phase transition for $J_1=-1.0$, $J_2=8.0$, $J_3=0.1$, $d=-10$, and $h_0=2.5$ and the initial values of $|M_\sigma|$ and $|M_S|$ are taken zero. This figure corresponds to the p phase.

of the mixed spin-1/2 and spin-5/2 [47], mixed spin-1 and spin-5/2 [48], mixed spin-3/2 and spin-5/2 ferrimagnetic system [49], the mixed spin Ising systems on Bethe lattice [50], the mixed spin-1/2 and spin-S Ising model on a bathroom tile (4–8) lattice [51], and also dynamic phase diagrams of the mixed spin-1/2 and spin-5/2 [52]. We should also mention that these dynamic phase diagrams are new phase diagrams, which have been obtained in this system.

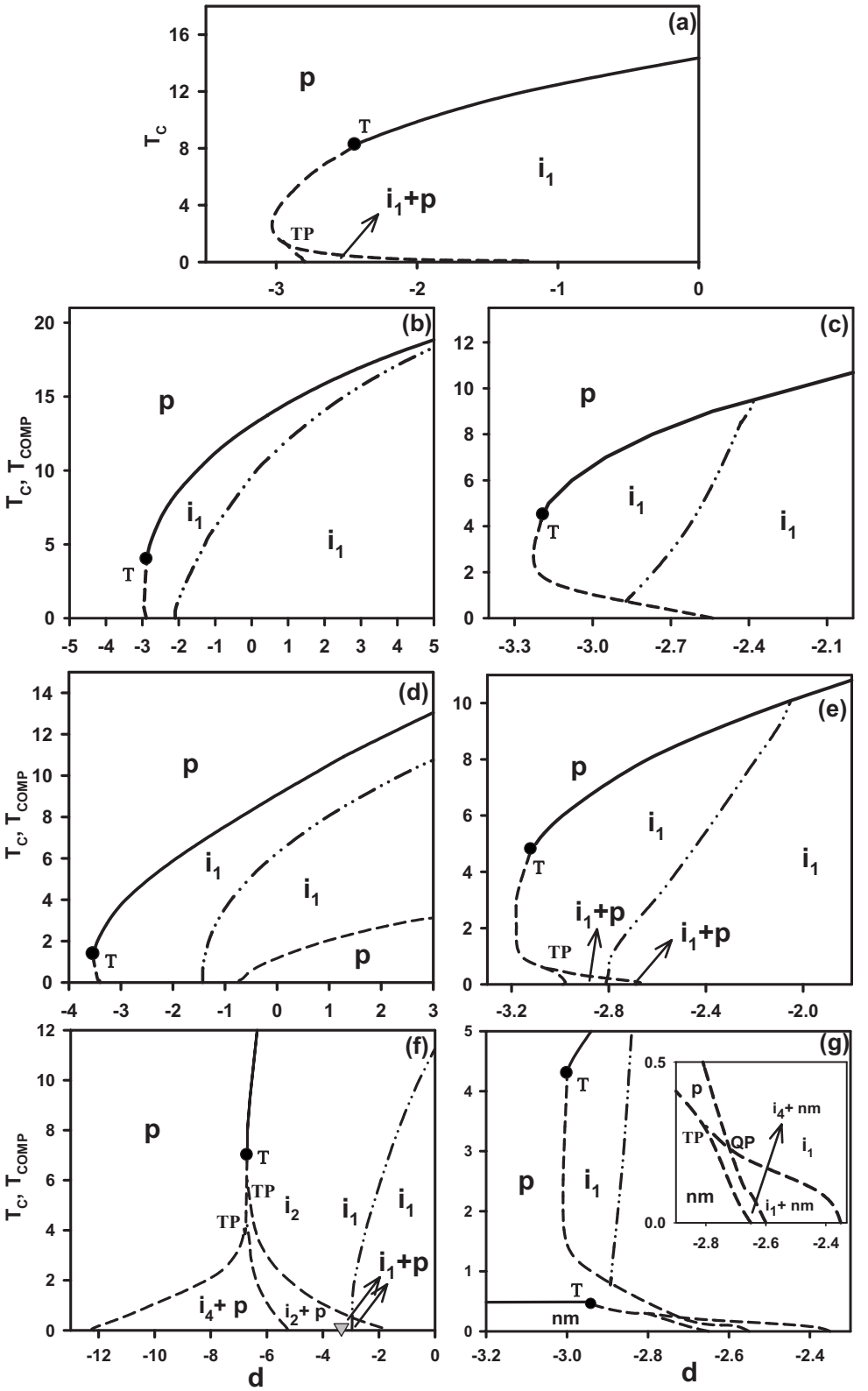

FIG. 4. Dynamic phase diagrams of the mixed spin-2 and spin-5/2 Ising ferrimagnetic model in the (d,T) plane. Dashed and solid lines are the dynamic first- and second-order phase boundaries, respectively. The dash-dot-dot line illustrates the compensation temperatures. The special points are the dynamic tricritical point with filled circle, the dynamic triple point (TP) and the dynamic quadruple point (QP). The filled triangle separates the i_2 phase from the i_1 for high value of T and the i_2+p mixed phase from the i_1+p mixed phase for low value of T. (a) $J_1=-1.0$, $J_2=1.1$, $J_3=0.9$, and $h_0=0.1$, (b) $J_1=-1.0$, $J_2=15$, $J_3=0.1$, and $h_0=2.5$, (c) $J_1=-1.0$, $J_2=1.5$, $J_3=0.9$, and $h_0=1.0$, (d) $J_1=-1.0$, $J_2=2.0$, $J_3=0.8$, and $h_0=10$, (e) $J_1=-1.0$, $J_2=1.5$, $J_3=0.8$, and $h_0=2.5$, (f) $J_1=-1.0$, $J_2=6.0$, $J_3=0.95$, and $h_0=1.5$ and (g) $J_1=-1.0$, $J_2=1.1$, $J_3=0.9$, and $h_0=0.1$.

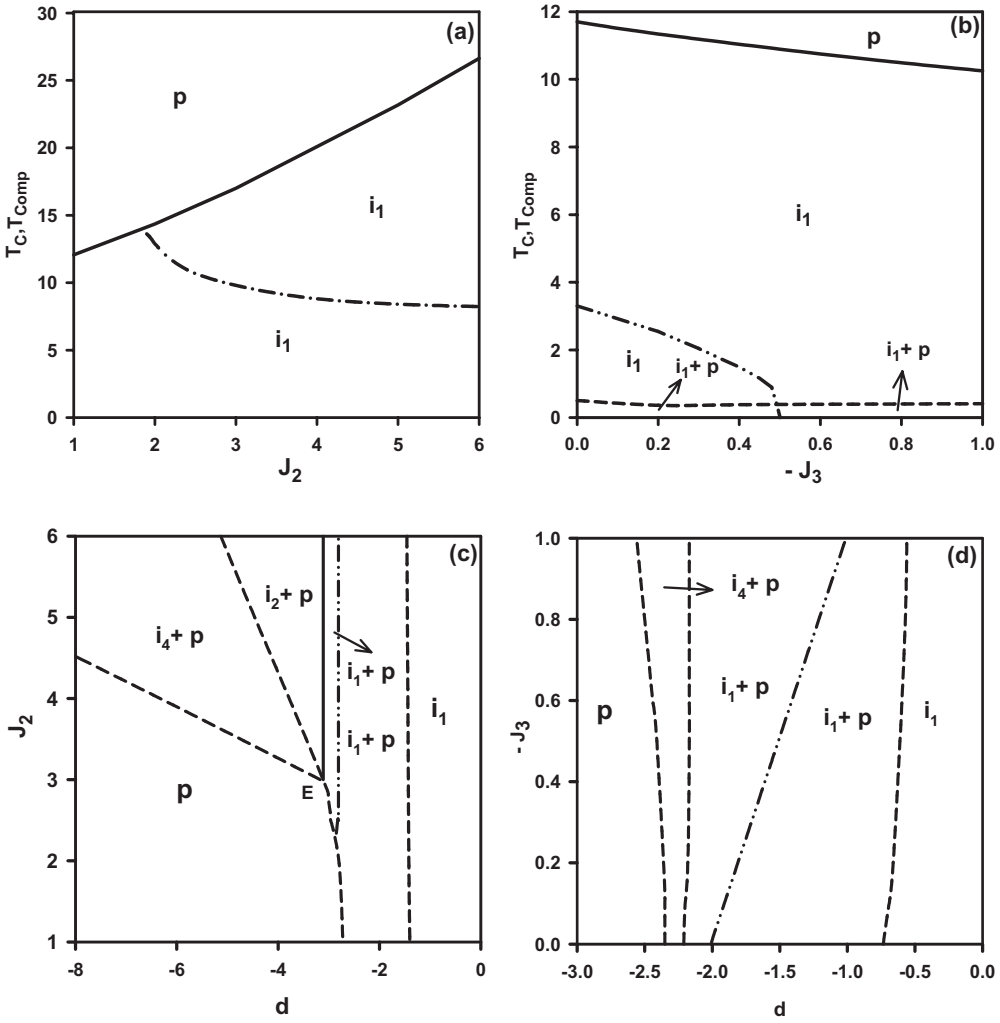

FIG. 5. Same as Fig. 4, but (a) In (J_2,T) plane for $J_1=-1.0$, $J_3=0.8$, $h_0=0.1$, and $d=-1.0$; (b) in $(-J_3,T)$ plane for $J_1=-1.0$, $J_2=2$, $h_0=0.1$, and $d=-1.50$; (c) in (d,J_2) plane for $J_1=-1.0$, $J_3=0.8$, $T=0.1$, and $h_0=1.0$, and (d) in $(d,-J_3)$ plane for $J_1=-1$, $J_2=2$, $h_0=0.1$, and $T=0.1$.

We also calculate the dynamic phase diagrams including the compensation behaviors in the (J_2,T), $(-J_3,T)$, (d,J_2), and $(d,-J_3)$ planes, and five, five, five, and two main topological different types of dynamic phase diagrams are found, respectively. Since the most of the phase diagrams in these planes can be readily obtained from the phase diagram in (d,T) plane, especially high and low values of d. We present only one interesting phase diagram that cannot be obtained readily from the phase diagrams in the (d,T) plane, in each plane, seen in Figs. 5(a)–5(d). The phase diagram is constructed for $J_1=-1$, $J_3=0.8$, $h_0=0.1$, and $d=-1.0$, and is presented in Fig. 5(a) that the system exhibits the p and i_1 fundamental phases. In this phase diagram, the dynamic phase boundary is only a second-order phase line, which separates the p phase from the i_1 phase. Figure 5(a) contains the compensation temperatures, but does not illustrate the dynamic tricritical behavior. The similar phase diagram with Fig. 5(a) was also obtained in the mixed spin-1/2 and spin-1 system [14,15]. Figure 5(b) shows the phase diagrams in the $(-J_3,T)$ plane for $J_1=-1$, $J_2=2$, $h_0=0.1$, and $d=-1.5$. In this phase diagram, the system exhibits one mixed phase, namely, i_1+p, besides the i_1 and p fundamental phases. The dynamic phase boundary between the i_1 and p is a second-order line and between the i_1 and i_1+p is first-order line. The phase diagram is presented for $J_1=-1$, $J_3=0.8$, $h_0=1$, and $T=0.1$, illustrated in Fig. 5(c). The phase diagram exhibits the i_1, p, i_1+p, i_2+p, and i_4+p phases. The dynamic phase boundaries among these phases are first-order lines, except the boundary between the i_1+p and i_2+p phases that is a second-order line. The system also exhibits the critical end point (E). Figure 5(d) shows the phase diagram for $J_1=-1$, $J_2=2$, $h_0=0.1$, and $T=0.1$ in the $(d,-J_3)$ plane. The system exhibits the i_1+p and i_4+p mixed phases, besides the i_1 and p fundamental phases. The dynamic phase boundaries among the phases are first-order phase lines. Thus, these phase diagrams of Figs. 5(b)–5(d) are only observed in this system.

IV. SUMMARY AND CONCLUSION

In this work, we have studied within a mean-field approach the stationary states of the kinetic mixed spin-2 and spin-5/2 Ising model in the presence of a time-dependent oscillating external magnetic field on a hexagonal lattice.

The lattice is formed by alternate layers of spins $\sigma=2$ and $S=5/2$. For this spin arrangement, any spin at one lattice site has two nearest-neighbor spins on the same sublattice, and four on the other sublattice. The Hamiltonian model includes the intersublattice interaction, intrasublattice interaction, crystal field interaction, and sinusoidal magnetic field. The intersublattice interaction is antiferromagnetic. We use the Glauber-type stochastic dynamics to describe the time evolution of the system. We have studied time variations in the average sublattice magnetizations in order to find the phases in the system and the temperature dependence of the average sublattice magnetizations in a period, which is also called the dynamic magnetizations, to obtain the dynamic phase transition points as well as to characterize the nature (continuous or discontinuous) of transitions. The total magnetization is also investigated as a function of temperature to find the compensation temperatures and to determine the type of behavior. Finally, dynamic phase diagrams are presented in two different planes. The phase diagrams contain the paramagnetic, the nonmagnetic, and three different ferrimagnetic fundamental phases, five different mixed phases, and the compensation temperature or the *N*-type behavior, depending on the interaction parameters. The system also displays the tricritical and re-entrant behaviors, which also strongly depend on interaction parameters. Moreover, in general, the dynamic boundary between the fundamental phases is a second-order line, but the boundary between the fundamental and mixed phases and also boundaries among the mixed phases are first-order lines.

The comparison of the present results with the results of the kinetic mixed spins (1/2, 3/2) Ising system [23] is as follows: (1) the mixed spins (2, 5/2) Ising system displays only *N*-type behavior, but the mixed spins (1/2, 3/2) Ising system exhibits both *P*-type and *L*-type behaviors [44,45]. *P*-type dependence shows the temperature-induced maximum as the temperature raises, whereas the *N*-type curve is being characterized by one compensation point at which resultant magnetization disappears due to the complete cancellation of the sublattice magnetization. The *L*-type curve [53] is very analogous to the *P*-type dependence, however, the resultant magnetization starts from zero in this particular case. (2) The mixed spins (2, 5/2) system contains seven mixed phases, besides six fundamental phases, but the mixed spins (1/2, 3/2) contains three mixed phases, besides three fundamental phases. (3) The mixed spins (2, 5/2) system exhibit the dynamic quadruple point, the triple point, and the critical end point, but the mixed spins (1/2, 3/2) does not. (4) The mixed spins (2, 5/2) system exhibits a re-entrant behavior, but the spins (1/2, 3/2) system does not. (5) The mixed spins (2, 5/2) Ising system has more main topological different types of phase diagrams than the spins (1/2, 3/2) system. On the other hand, the main differences between the kinetic mixed spins (2, 5/2) and spins (1/2, 1) [14,15] Ising systems are as follows: (1) both system display *N*-type behavior. (2) The mixed spins (2, 5/2) and spins (1/2, 1) [15] Ising systems exhibit a dynamic tricritical and a re-entrant behaviors. (3) The mixed spins (2, 5/2) Ising system displays more fundamental phase diagrams than the spins (1/2, 1) [14,15] system. (4) The mixed spins (2, 5/2) system contains seven mixed phases, besides six fundamental phases, but the mixed spins (1/2, 1) [15] contains three mixed phases, besides three fundamental phases. (5) The mixed spins (2, 5/2) system exhibits the QP, TP, and E special points, but the mixed spins (1/2, 1) [15] exhibits only the dynamic multicritical (A) and the dynamic double critical end (B) special points. Therefore, from these comparisons one can see that the mixed spins (2, 5/2) Ising system gives more richer phase diagrams than the mixed Ising systems with spins (1/2, 1) and with spins (1/2, 3/2).

Finally, we should also mention that this mean-field dynamic study, in spite of its limitations such as the correlation of spin fluctuations have not been considered, suggests that kinetic mixed spin-2 and spin-5/2 Ising model has an interesting dynamic behavior and gives rich dynamic phase diagrams. Hence, we hope that our detailed theoretical investigation may stimulate further works to study the nonequilibrium or the dynamic phase transition in the kinetic mixed spins (2, 5/2) Ising system by using nonperturbative methods such as kinetic Monte-Carlo (MC) simulations or renormalization-group calculations. We also mention that some of the first-order lines and some of the tricritical and the other special points might be artifacts of the mean-field calculation. This fact has been discussed extensively in the kinetic spin-1/2 Ising model in recent works [54–56]; hence, this system should be studied by using nonperturbative methods in order to find the artifacts in the first-order phase lines and the tricritical points. Moreover, our results will be instructive for the time-consuming process of the dynamic nonperturbative calculations, such as the dynamic MC simulations, which consequently can short the dull process of searching the critical behavior while using the dynamic MC.

ACKNOWLEDGMENTS

This work was supported by the Scientific and Technological Research Council of Turkey (TÜBİTAK) under Grant No. 107T533 and Erciyes University Research Fund under Grant No. FBA-06-01. We are grateful to Bayram Deviren for useful discussions.

APPENDIX: THE VALUES OF $W_i^\sigma(\sigma_i \rightarrow \sigma_i')$

The probabilities $W_i^\sigma(\sigma_i \rightarrow \sigma_i')$ in Eq. (4) are calculated as follows:

$$W_i^\sigma(2 \rightarrow 0) = W_i^\sigma(1 \rightarrow 0) = W_i^\sigma(-1 \rightarrow 0) = W_i^\sigma(-2 \rightarrow 0) = W_i^\sigma(0) = \frac{1}{\tau} \frac{1}{2\exp(\beta D)\cosh(\beta x) + 2\exp(4\beta D)\cosh(2\beta x) + 1},$$

$$W_i^\sigma(2 \rightarrow 1) = W_i^\sigma(0 \rightarrow 1) = W_i^\sigma(-1 \rightarrow 1) = W_i^\sigma(-2 \rightarrow 1) = W_i^\sigma(1) = \frac{1}{\tau} \frac{\exp(\beta x)\exp(\beta D)}{2\exp(\beta D)\cosh(\beta x) + 2\exp(4\beta D)\cosh(2\beta x) + 1},$$

$$W_i^{\sigma}(1 \to 2) = W_i^{\sigma}(0 \to 2) = W_i^{\sigma}(-1 \to 2) = W_i^{\sigma}(-2 \to 2) = W_i^{\sigma}(2) = \frac{1}{\tau} \frac{\exp(2\beta x)\exp(4\beta D)}{2\exp(\beta D)\cosh(\beta x) + 2\exp(4\beta D)\cosh(2\beta x) + 1},$$

$$W_i^{\sigma}(1 \to -1) = W_i^{\sigma}(2 \to -1) = W_i^{\sigma}(0 \to -1) = W_i^{\sigma}(-2 \to -1) = W_i^{\sigma}(-1) = \frac{1}{\tau} \frac{\exp(-\beta x)\exp(\beta D)}{2\exp(\beta D)\cosh(\beta x) + 2\exp(4\beta D)\cosh(2\beta x) + 1},$$

$$W_i^{\sigma}(2 \to -2) = W_i^{\sigma}(1 \to -2) = W_i^{\sigma}(0 \to -2) = W_i^{\sigma}(-1 \to -2) = W_i^{\sigma}(-2) = \frac{1}{\tau} \frac{\exp(-2\beta x)\exp(4\beta D)}{2\exp(\beta D)\cosh(\beta x) + 2\exp(4\beta D)\cosh(2\beta x) + 1},$$

where $x = J_1 \Sigma_j S_j + J_2 \Sigma_j \sigma_j + H$.

[1] G. M. Zhang and C. Z. Yang, Phys. Rev. B **48**, 9452 (1993).
[2] T. Kaneyoshi, Phys. Rev. B **55**, 12497 (1997).
[3] G. M. Buendía and M. A. Novonty, J. Phys.: Condens. Matter **9**, 5951 (1997).
[4] J. W. Tucker, J. Magn. Magn. Mater. **195**, 733 (1999).
[5] A. P. Vieira, J. X. de Carvalho, and S. R. Salinas, Phys. Rev. B **63**, 184415 (2001).
[6] G. M. Buendía and E. Machado, Phys. Rev. E **58**, 1260 (1998).
[7] M. Godoy and W. Figueiredo, Phys. Rev. E **61**, 218 (2000); **65**, 026111 (2002); **66**, 036131 (2002).
[8] E. Albayrak and M. Keskin, J. Magn. Magn. Mater. **261**, 196 (2003).
[9] C. Ekiz and M. Keskin, Physica A **317**, 517 (2003); M. Keskin, O. Canko, and Y. Polat, J. Korean Phys. Soc. **53**, 497 (2008).
[10] T. Kasama, Y. Muraoka, and T. Idogaki, Phys. Rev. B **73**, 214411 (2006).
[11] L. Bahmad, A. Benyoussef, and A. El Kenz, Physica A **387**, 825 (2008).
[12] Y. F. Zhang and S. L. Yan, Phys. Lett. A **372**, 2696 (2008).
[13] Y. Belmamoun and M. Kerouad, Phys. Scr. **77**, 025706 (2008).
[14] M. Godoy, V. S. Leite, and W. Figueiredo, Phys. Rev. B **69**, 054428 (2004).
[15] M. Keskin and M. Ertaş, J. Stat. Phys. (to be published).
[16] N. Benayad, A. Dakhama, A. Klümper and J. Zittartz, Z. Phys. B **101**, 623 (1996).
[17] G. M. Buendía and R. Cardona, Phys. Rev. B **59**, 6784 (1999).
[18] W. Jiang, G.-Z. Wei, and Z.-H. Xin, Physica A **293**, 455 (2001).
[19] G.-Z. Wei, Y.-Q. Liang, Q. Zhang, and Z.-H. Xin, J. Magn. Magn. Mater. **271**, 246 (2004).
[20] C. Ekiz, J. Magn. Magn. Mater. **293**, 913 (2005).
[21] Y.-Q. Liang, G.-Z. Wei, F.-C. Ma, and G.-L. Song, Physica A **387**, 4513 (2008).
[22] B. Deviren, M. Keskin, and O. Canko, J. Magn. Magn. Mater. **321**, 458 (2009).
[23] M. Keskin, B. Deviren, and O. Canko, IEEE Trans. Magn. **45**, 2640 (2009)
[24] A. Bobák and M. Jurčišin, Phys. Status Solidi B **204**, 787 (1997).
[25] J. W. Tucker, J. Magn. Magn. Mater. **237**, 215 (2001).
[26] Y. Nakamura and J. W. Tucker, IEEE Trans. Magn. **38**, 2406 (2002)
[27] W. Jiang, G.-Z. Wei, and Z.-D. Zhang, Phys. Rev. B **68**, 134432 (2003).
[28] C. Ekiz, J. Magn. Magn. Mater. **307**, 139 (2006).
[29] E. Albayrak and T. Bulut, Physica B **400**, 124 (2007).
[30] M. Keskin, E. Kantar, and O. Canko, Phys. Rev. E **77**, 051130 (2008).
[31] T. Kaneyoshi, Y. Nakamura, and S. Shin, J. Phys.: Condens. Matter **10**, 7025 (1998); Y. Nakamura, S. Shin, and T. Kaneyoshi, Physica B **284–288**, 1479 (2000).
[32] Y. Nakamura, J. Phys.: Condens. Matter **12**, 4067 (2000).
[33] Y. Nakamura, Prog. Theor. Phys. **138**, 466 (2000).
[34] Y. Nakamura, Phys. Rev. B **62**, 11742 (2000).
[35] J. Li, A. Du, and G. Wei, Phys. Status Solidi B **238**, 191 (2003).
[36] J. Li, A. Du, and G. Wei, Physica B **348**, 79 (2004).
[37] J. Li, A. Du, and G. Wei, Phys. Status Solidi B **240**, 610 (2003).
[38] G. Z. Wei, Q. Zhang, Z. Xin, and Y. Liang, J. Magn. Magn. Mater. **277**, 1 (2004).
[39] G. Wei, Q. Zhang, J. Zhao, and Y. Gu, Physica B **381**, 6 (2006).
[40] E. Albayrak, Physica A **375**, 174 (2007); A. Yigit and E. Albayrak, J. Magn. Magn. Mater. **309**, 87 (2007); Phys. Lett. A **372**, 361 (2008).
[41] R. J. Glauber, J. Math. Phys. **4**, 294 (1963).
[42] R. R. Netz and A. N. Berker, Phys. Rev. B **47**, 15019 (1993).
[43] C. Ekiz and M. Keskin, Phys. Rev. B **66**, 054105 (2002).
[44] L. Néel, Ann. Phys. **3**, 137 (1948).
[45] S. Chikazumi, *Physics of Ferromagnetism* (Oxford University Press, Oxford, 1997).
[46] A. H. Cooke, C. J. Ellis, K. A. Gehring, M. J. M. Leask, D. M. Martin, B. M. Wanklyn, M. R. Wells, and R. L. White, Solid State Commun. **8**, 689 (1970); A. H. Cooke, D. M. Martin, and M. R. Wells, *ibid.* **32**, C1 (1971).
[47] B. Deviren, M. Keskin, and O. Canko, Physica A **388**, 1835 (2009).
[48] B. Deviren, M. Batı, and M. Keskin, Phys. Scr. **79**, 065006 (2009).
[49] Q. Zhang, G. Wei, and Y. Gu, Phys. Status Solidi B **242**, 924 (2005).
[50] E. Albayrak and A. Yigit, Phys. Lett. A **353**, 121 (2006).
[51] J. Strečka, Physica A **360**, 379 (2006).

[52] B. Deviren, M. Keskin, and O. Canko, Commun. Theor. Phys. (to be published).
[53] B. Barbara, D. Gignoux, and C. Vettier, *Lectures on Modern Magnetism* (Springer-Verlag, Berlin, 1998).
[54] M. Acharyya, Phys. Rev. E **59**, 218 (1999).
[55] G. Korniss, P. A. Rikvold, and M. A. Novotny, Phys. Rev. E **66**, 056127 (2002).
[56] M. Acharyya and A. B. Acharyya, Commun. Comput. Phys. **3**, 397 (2008).